ELSEVIER

Journal of Arid Environments 62 (2005) 677–700

Journal of Arid Environments

www.elsevier.com/locate/jnlabr/yjare

Inter-annual variability and interaction of remote-sensed vegetation index and atmospheric precipitation in the Aral Sea region

N.P. Nezlin[a,*], A.G. Kostianoy[b], Bai-Lian Li[c]

[a]*Southern California Coastal Water Research Project (SCCWRP), 7171 Fenwick Lane, Westminster, CA 92683, USA*

[b]*P. P. Shirshov Institute of Oceanology of Russian Academy of Sciences, 36 Nakhimovskiy Prospekt, Moscow 117851, Russia*

[c]*Department of Botany & Plant Sciences, University of California Riverside (UCR), Riverside, CA 92521, USA*

Received 29 August 2002; received in revised form 20 October 2004; accepted 18 January 2005
Available online 11 March 2005

Abstract

The remotely sensed Normalized Difference Vegetation Index (AVHRR NDVI) and precipitation data were analysed in the Aral Sea region in Central Asia during two recent decades. Both variables exhibited pronounced seasonal variation, with maximum precipitation in March and maximum NDVI in May–June. The regions of synchronous seasonal and inter-annual variability between the vegetation index and precipitation were distinguished using the Empirical Orthogonal Functions (EOF) method and time-lagged correlations between EOF modes. At a seasonal scale, precipitation and the vegetation index were correlated with a time lag from 1 to 6 months in different regions with peak plant growth following precipitation maxima.

Keywords: Satellite data analysis; NDVI; Precipitation; Aral Sea; Desertification

*Corresponding author. Tel.: +1 714 372 9227; fax: +1 714 894 9699.

E-mail addresses: nikolayn@sccwrp.org (N.P. Nezlin), kostianoy@mail.mipt.ru (A.G. Kostianoy), bai-lian.li@ucr.edu (Bai-Lian Li).

0140-1963/$ - see front matter © 2005 Elsevier Ltd. All rights reserved.
doi:10.1016/j.jaridenv.2005.01.015

1. Introduction

Satellite imagery is a convenient tool for global monitoring of terrestrial ecosystems; it enables regular detection of seasonal and inter-annual changes in vegetation biomass (Tarpley et al., 1984; Tucker et al., 1985; Pinker and Laszlo, 1992). The Advanced Very High Resolution Radiometer (AVHRR) onboard the National Oceanic and Atmospheric Administration's (NOAA) polar orbiting satellites has the longest record of research (Cracknell, 1997), exceeding two decades. Several vegetation indices have been developed to measure the state of vegetation from orbital platforms, based on combinations of two or more spectral bands (Gutman, 1991; Bannari et al., 1995; Gobron et al., 2000; Gitelson et al., 2002). These indices are correlated with various parameters characterizing the level of vegetation dynamics, such as chlorophyll concentration (Buschmann and Nagel, 1993), photosynthesis (Sellers, 1985), carbon fluxes (Tucker et al., 1986), evapotranspiration (Cihlar et al., 1991), green biomass and coverage (Tucker, 1979; Tucker et al., 1983, 1985; Elvidge and Chen, 1995), agricultural crops (Rasmussen, 1997), etc.

The most widely used vegetation index for agricultural and ecological applications is the Normalized Difference Vegetation Index (NDVI), introduced in 1970s (Rouse et al., 1974). It is based on the general idea that chlorophyll pigments in leaves absorb solar radiation in the visible part of the spectrum and strongly reflect and backscatter radiation in the near-infrared band. AVHRR radiometer observes the earth in visible (VIS) and near-infrared (NIR) channels (VIS = 0.55–0.68 μm; NIR = 0.73–1.10 μm). This allows one to assess differences in vegetation on a global scale. NDVI is defined as NDVI = (NIR−VIS)/(VIS + NIR), which ranges from <0.02 for deserts to >0.5 for fully developed canopies.

NDVI provides an appropriate tool for the analysis of vegetation at a wide range of spatial scales, from 1 to >500 km resolution (Justice et al., 1991). Attempts have been made to use the AVHRR data for long-term monitoring of terrestrial reflectance values and vegetation indices (Gutman, 1999; Kaufman et al., 2000). These and other studies on long-term monitoring are motivated by the availability of quality AVHRR time-series for the period of nearly 20 years.

The goal of this study is to analyse the seasonal and inter-annual variations of NDVI in the region surrounding the Aral Sea, and to explore relationships with contemporary variation in precipitation. In analysing NDVI patterns, we keep in mind that NDVI is statistically correlated to vegetation but does not provide an evidence for a distinct level of vegetation biomass and/or the presence of specific vegetation types.

2. The Aral Sea region

The Aral Sea is a terminal lake (no outflow) located in Central Asia (Fig. 1). It receives inflow from two rivers only: Amu Darya and Syr Darya. The surface area of the Aral Sea was 68,320 km^2 in 1960, making it the fourth largest inland water body

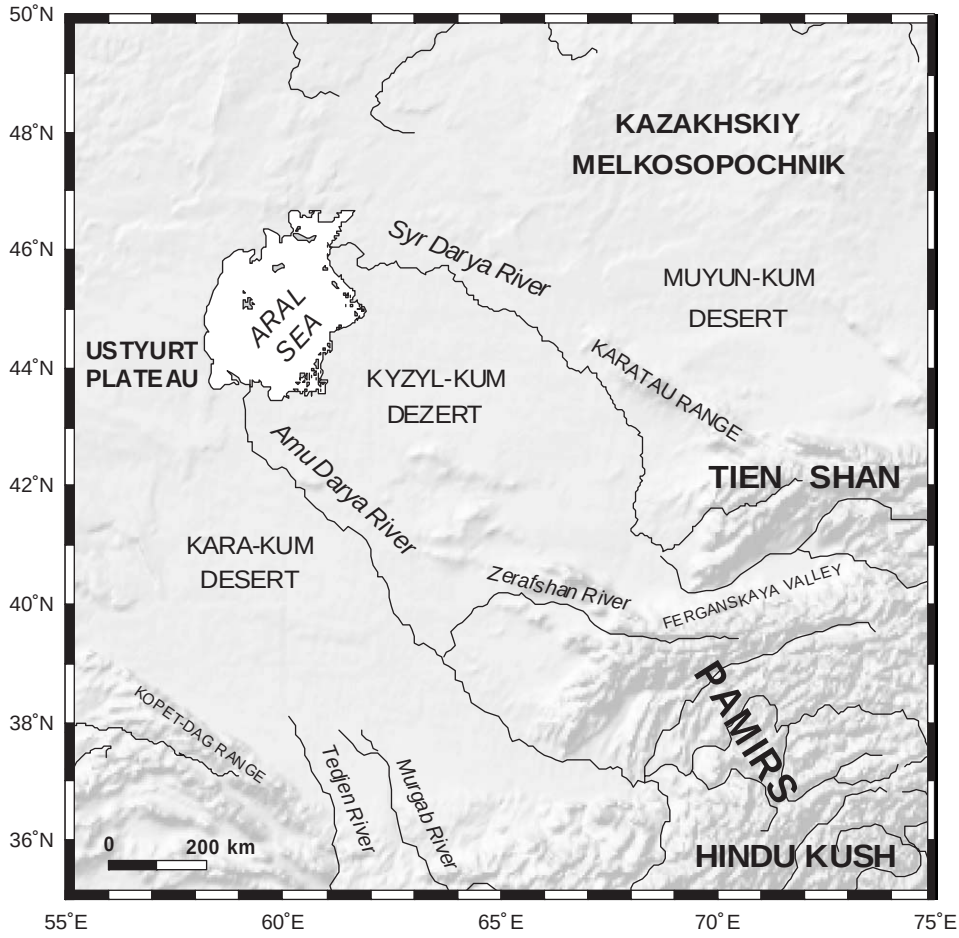

Fig. 1. The Aral Sea region.

on Earth. It existed in that form during the past 8–10 thousand years (Boomer et al., 2000).

Amu Darya is the most important river within the Aral Sea basin (Froebrich and Kayumov, 2004). Originating among glaciers and snowfields of the Pamir Mountains of Tajikistan, Kyrgyzstan, and Afghanistan, it flows nearly 2400 km from the mountains across the Kara-Kum Desert and into the Aral Sea. Average annual flow from the drainage basin is around 79 km^3 (Micklin, 2000). This includes not only the flow of the Amu Darya and its tributaries but also several ''terminal'' rivers (Zeravshan, Murgab, Tedjen) that disappear in the deserts.

The flow of the Amu Darya is substantially diminished by evaporation, transpiration from vegetation along its banks, and bed filtration as the river passes across the Kara-Kum Desert to the Aral Sea. Even prior to the development of

modern large-scale irrigation, average inflow of the river to the Aral Sea was around 40 km^3, compared to 62 km^3 coming from the mountains (Micklin, 2000).

The Syr Darya River flows from the Tien Shan Mountains, located to the north of the Pamirs. It is chiefly fed by glaciers and snowmelt. Its total length is 2500 km. The average annual flow of the Syr Darya River is 37 km^3 (Micklin, 2000). Similar to Amu Darya, even prior to modern age of irrigation, the loss of Syr Darya flow was substantial during its long journey across the Kyzyl-Kum Desert, with less than half (around 15 km^3 on the average annual basis) of the water coming from the mountains reaching the Aral Sea.

The Aral Sea area is classified as an "Arid-Temperate Climate" zone (Walter, 1985; West, 1983). The main part of this zone is covered by dry "feather-grass" steppes, semi-deserts, and deserts. In semi-deserts the plant cover consists mainly of shrubs, especially the genus *Artemisia*. In deserts, ground is covered only in spring with ephemeral plants. Total phytomass there is very small (<5 t/ha); at the same time the delta of the Amu Darya supports luxuriant *Populus–Halimodendron* forests rich in lianas, as well as large expansion of reeds (*Phragmites*), with total phytomass as high as 77.8 t/ha (Walter, 1985).

Cold winter, on the one hand, and drought of late summer, on the other, limit the growing season to a few months in spring and early summer. The total leaf area developing during this period varies greatly from year to year according to rainfall. In the plain area around the Aral Sea, cyclonic rain is still received from the Atlantic Ocean, falling in the winter in the southern parts, and mostly in the spring in the north; in any case, the soil here is always wet in spring after the snows have melted. The winters are cold, hence evaporation during this season is very small. In summer, potential evaporation is 10–15 times precipitation due to hot and dry weather (Walter, 1985).

After 1957, the Aral Sea began to dry up as more and more water was directed to irrigate cotton and other crops. In the past, the sea received 50–60 km^3 of water a year from its two main feeder rivers, but by the mid-1980s, river flow into the sea had shrunk to 2–5 km^3 a year (Keyser et al., 1999; Jarsjo and Destouni, 2004). As a result of the reduced inflow, the water balance of the Aral Sea became negative after 1960; evaporation from the lake surface was greater than the sum of the on-lake precipitation and the reduced stream flow. As a result, the lake surface area decreased ~60%, the mean depth decreased from 15 to 8 m, the water volume decreased by 80%, and salinity increased from 10 to >35 ppt (Small et al., 2001b). Desiccation has weakened the "lake effect" of the Aral Sea, influencing climate over a distance of several hundred kilometers (Khan et al., 2004); air temperature near the Aral Sea changed up to 6 °C (Small et al., 2001a).

The dramatic changes in the Aral Sea hydrology inevitably resulted in the changes of land vegetation. The process of desertification implies the diminution or destruction of the biological potential of land (Biswas and Biwas, 1980). We define desertification as a transition from land areas covered by a dense vegetation canopy to deserts with scarce plants. Unfortunately, the satellite-born NDVI record (starting from 1981) is too short to reveal the entire process of the shrinking terrestrial vegetation around the Aral Sea, which has been occurring at a large scale since the

1960s. However, it is important to discern the difference between the catastrophic anthropogenic impacts we observed around the Aral Sea and natural trends in climate change, including changes in precipitation.

3. Data and method used for analysis

The NDVI data were obtained from the NASA Goddard Space Flight Center Distributed Active Archive Center (GSFC DAAC). The monthly NDVI maps of $1^\circ \times 1^\circ$ latitude and longitude resolution were derived from the five-channel cross-track scanning AVHRR aboard the NOAA Polar Orbiter "afternoon" satellites (NOAA-7, -9, -11 and -14). The data span the period from July 1981 till September 2001, with a data gap in September–December 1994 due to satellite failure.

Precipitation information from the Aral Sea area was obtained from the data collected and processed at the Global Precipitation Climatology Centre (GPCC) in Germany. The GPCC products are gridded datasets of monthly total precipitation derived from observed data measured by rain gauges. These products cover the entire earth's land surface. The spatial resolution is $1^\circ \times 1^\circ$ geographical latitude and longitude. The GPCC rainfall data are based on completely quality-controlled data from globally exchanged synoptic weather reports and monthly climate reports from 6000 to 7000 stations all over the world. The data were interpolated to area-means at GPCC using the empirical weighting scheme SYMAP designed by Shepard (1968) and modified by Willmott et al. (1985). In this method the monthly precipitation amounts measured locally at stations were interpolated on a 0.5° grid. Area-means of 0.5° grid cells are calculated as arithmetic means of the interpolated data from the four corners of the cell. Area-means on 2.5° or 1° grid cells were calculated from means of all embraced 0.5° grid cells weighted with the portion of land-coverage (Rudolf et al., 1992). This methodology does not take into account spherical trigonometry in its area-based weighting calculations and as such, the grids produced by GPCC are smoother in the equatorial regions and less so in the polar zones due to the anisotropic weightings.

We used GPCC data for the period from January 1986 to November 2001. Spatial coverage of NDVI and GPCC subsets analysed in this study was 35–50°N and 55–74°E. Hereafter we use abbreviations NDVI and GPCC to indicate monthly global vegetation index from NASA archive and monthly global atmospheric precipitation data from GPCC archive.

To illustrate spatial distribution of NDVI and GPCC over the study area, each parameter in each $1^\circ \times 1^\circ$ grid node was averaged over the entire period of observations (1981–2001 for NDVI and 1986–2001 for GPCC). Temporal variability of NDVI and GPCC in each $1^\circ \times 1^\circ$ grid node was characterized by standard deviation (SD) estimated using conventional statistical method. Then monthly climatological maps of NDVI and GPCC were composed by averaging the data for each month (January, February, etc.) over the entire observation periods in each $1^\circ \times 1^\circ$ grid node. These interpolated data were then subtracted from the actual data to produce NDVI and GPCC seasonal anomalies.

To analyse the spatio-temporal variability of NDVI and GPCC anomalies in the entire study region, we used the statistical method of Empirical Orthogonal Functions (EOF). This statistical approach is a convenient method for the analysis of successive patterns of data distributed in space. The EOF method decomposes space and time-distributed data into modes ranked by their temporal variance. A mathematically similar statistical method (Principle Component Analysis) was applied to NDVI images earlier for other purposes, e.g. for classification of vegetation types (Tucker et al., 1985) and the analysis of change vectors in the multi-temporal space (Lambin and Strahler, 1994).

The methodology of EOF is described in detail in Priesendorfer (1988). Each grid of observations (NDVI or GPCC anomalies) is converted into a vector of the matrix **T** with dimension $M \cdot N$, where M is the number of spatially distributed points, i.e. the number of grid nodes, and N is the number of observations over time (i.e. grids). The matrix **T** was then decomposed into two additional matrices as follows: $\mathbf{T} = \mathbf{A} \cdot \mathbf{B}$, where **A** is $M \cdot I$ matrix and **B** is $I \cdot N$ matrix, with I being the number of nonzero EOF modes. Taking into account the percentage of explained variance, modes with eigenvalues >1 are considered significant. Then each vector of matrix **A** is converted into a grid representing the contribution of this mode into different areas of the region. The corresponding vector of **B** matrix was analysed using a Fourier transform method to reveal the temporal scale of variations, with focus on seasonal and inter-annual changes. The correlation functions between different EOF modes of NDVI and GPCC were estimated to analyse the time-lagged relationships between these parameters.

4. Results

4.1. General distribution and seasonal cycles of NDVI and GPCC

The spatial distribution of NDVI averaged over the entire period of observations (July 1981–September 2001) is shown at Fig. 2a. The NDVI values vary from 0.02 to 0.3. NDVI values are lowest to the southwest of the Aral Sea (the Ustyurt Plateau), in the desert areas Kara Kum and Kyzyl Kum, and in the zone of Pamir Mountains. Low values of NDVI are observed in the latitudinal zone along 45°–46°N, i.e. from the Aral Sea to the northern part of Muyunkum Desert. To the north of 45°–46°N NDVI gradually increases. High NDVI values were found in the Ferganskaya Valley and on the western slopes of Tien Shan and Pamir Mountains (i.e. in the upper courses of Amu Darya and Syr Darya Rivers and their tributaries). High levels of the NDVI vegetation index were also evident in the southern part of the study region, along Kopet-Dag Range and in the basins of Tedjen and Murgab Rivers. High NDVI indicates dense vegetation in the lower course of Amu Darya River near the Aral Sea. At the same time, along the lower course of Syr Darya River NDVI is low.

Figure 2b illustrates the variability of NDVI. In general, the zones of high NDVI variability coincide with the zones of high total values of NDVI. Nevertheless, some differences are evident. The highest variation in NDVI (>0.2) was located in the

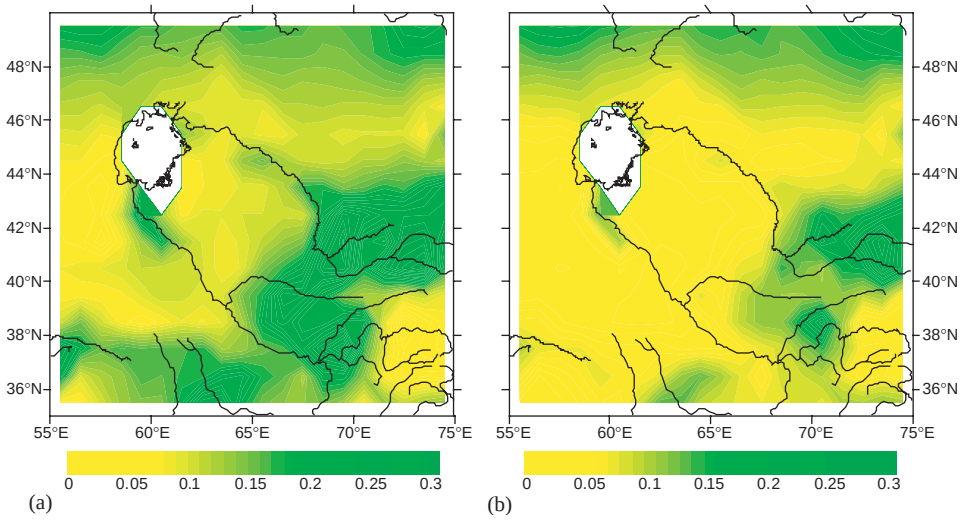

Fig. 2. Distribution of mean (a) and standard deviation (b) of NDVI averaged over July 1981–September 2001.

mountain regions of Tien Shan and western Pamirs, and in the northernmost zone of the study region. This was attributed to pronounced seasonality; during winter snow completely covers the vegetation. In other zones of high NDVI (Kopet-Dag Range, the basins of Tedjen and Murgab Rivers, lower course of Amu Darya) the variation in NDVI is less pronounced (SD = 0.1–0.15), indicating less seasonality in more southern latitudinal zones.

Figure 3a illustrates the spatial distribution of atmospheric precipitation (GPCC) in the study region. The zones of high precipitation appear to correspond to zones of high NDVI values. Maximum precipitation (>30 mm/month) occurs in western Tien Shan, northern Pamir Mountains, and eastern Hindu Kush. Minimum precipitation occurs around the Aral Sea, in Kara-Kum and Kyzyl-Kum Deserts. The zone of high precipitation in the eastern Hindu Kush Mountains does not coincide with high vegetation index. Also, the zone of rather high NDVI in the lower course of Amu Darya (>0.2) coincides with the zone of extremely low precipitation (<10 mm/month). Evidently, Amu Darya River seems to be an exclusive source of water for the plants growing there. It is interesting that precipitation over the upper course of Syr Darya exceeds precipitation observed at the upper course of Amu Darya. Nevertheless, NDVI indicates dense vegetation in the zones near the Aral Sea fed by Amu Darya rather than Syr Darya (Fig. 2a). Spatial distribution of GPCC variability (Fig. 3b) reflects the spatial distribution of its total values, including minor details.

Figure 4 illustrates the seasonal cycles of GPCC and NDVI averaged over the entire study region. Minimum of GPCC (<10 mm/month) occurs in August–September. Then precipitation gradually increases until March with a maximum

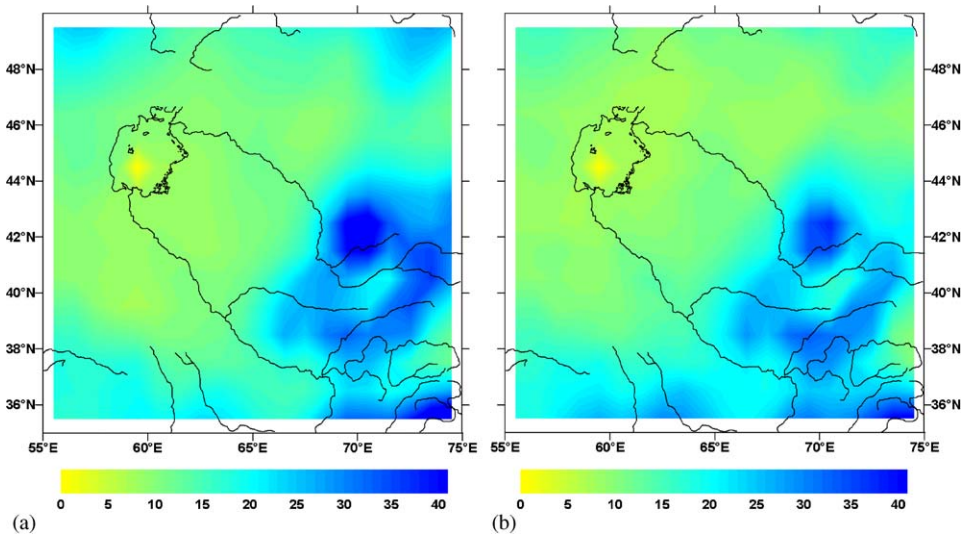

Fig. 3. Distribution of mean (a) and standard deviation (b) of precipitation averaged over January 1986–November 2001. Units of color scale are (mm/month).

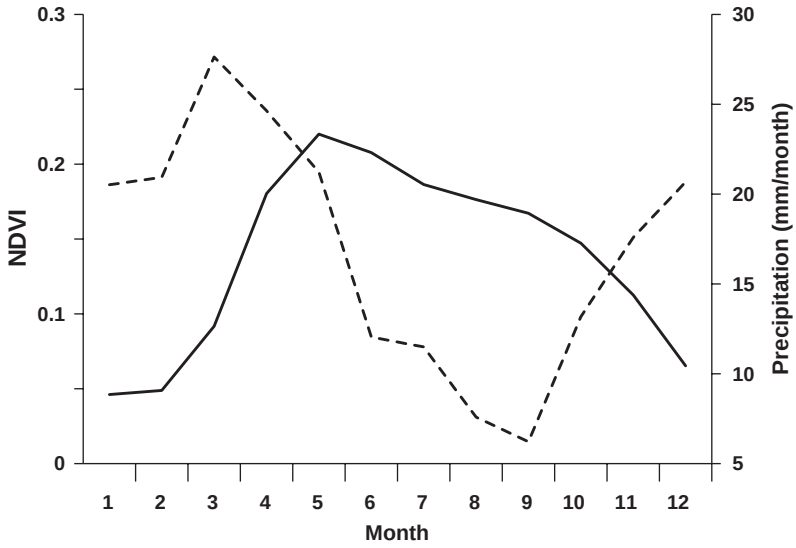

Fig. 4. Climatic seasonal variations of NDVI (solid line, left *Y*-axis) and precipitation (dashed line, right *Y*-axis) averaged over the entire study region (35°–50°N, 55°–75°E).

>25 mm/month; it then abruptly falls to 12 mm/month in June. The NDVI maximum occurs a few months later (in May) than precipitation maximum and is less pronounced. The minimum vegetation index (about 0.05) occurs during winter

(December–February). Then NDVI increases to 0.2 in April and the NDVI high remains until late autumn. When analysing the seasonal patterns, we expected that the NDVI maximum could lag the peak of vegetation biomass, because dormant, senescent, and even dead plants in summer significantly contribute to the spectral reflectance of grass canopy (Tucker, 1978).

The water balance of the Aral Sea region is estimated as 133 km^3/year (Micklin, 2000). This value results from 116 km^3 in Amu Darya, Syr Darya, and terminal rivers in the basin of Amu Darya, and 17 km^3 in ground-waters. Assuming the Aral Sea basin area to be 1.8 million km^2 (Micklin, 2000), we conclude that total atmospheric precipitation contributes about 350 km^3 of water per year. Less than 50% of this water feeds river flows and ground-waters, more than one-half returning into the atmosphere with evaporation.

4.2. Spatio-temporal variability of vegetation index (NDVI) and atmospheric precipitation (GPCC) anomalies

Hereafter we analyse NDVI and GPCC anomalies, i.e. the differences between actual total values and monthly averaged climate data in every $1^\circ \times 1^\circ$ data pixel. These anomalies were converted into the **T** matrix (300 pixels $\times$ 239 observations for NDVI and 300 pixels $\times$ 191 observations for GPCC), which was decomposed into two additional matrices (see the methodology section). Four leading EOF modes were selected for the analysis of both NDVI and GPCC; the reason for the retention of four modes was that the spatial distribution and temporal variation of these modes yield reasonable explanations.

Figure 5 illustrates spatial distribution of the four leading NDVI EOF modes. The first EOF mode explains $>14\%$ of total NDVI variability. It is associated with high NDVI in the northern part of the study region and low NDVI in the upper courses of Amu Darya and Syr Darya Rivers. Time-series analysis reveals slight decreasing trend (Table 1) and temporal periodicity of 4–5 years (Fig. 6a). Minima of the first EOF mode occurred in 1985, 1991, 1995, and 1999; maxima in 1989, 1993, 1997, and 2000. The long (2.5 years) persistent period of negative values starting from the beginning of 1998 is noteworthy.

The second EOF mode explains 10.2% of NDVI variability. It is associated with a high vegetation index in the mountains, especially in the upper course of Syr Darya, excluding Ferganskaya Valley. Maximum of temporal periodicity is one year (Fig. 6b), i.e. the second EOF mode is associated with residual seasonal variability. Time-series of the second EOF mode exhibits slight trend toward increase (Table 1; Fig. 6b); this trend is especially evident from 1980 to 1987. Then the second EOF mode decreases by 1993, and then increases by 1996. In 1996–1997 a persistent period of positive EOF values occurred, followed by a dramatic decrease by mid-1998 and a new increase by 2000.

The third NDVI EOF mode explains 7.0% of variability. The maximum is located in the catchment area of Syr Darya, in the Muyunkum Desert, and to the northwest of the Aral Sea; minimum is in the upper course of Amu Darya and the basins of Tedjen and Murgab Rivers. Linear trend is almost zero (Table 1; Fig. 6c). Fourier

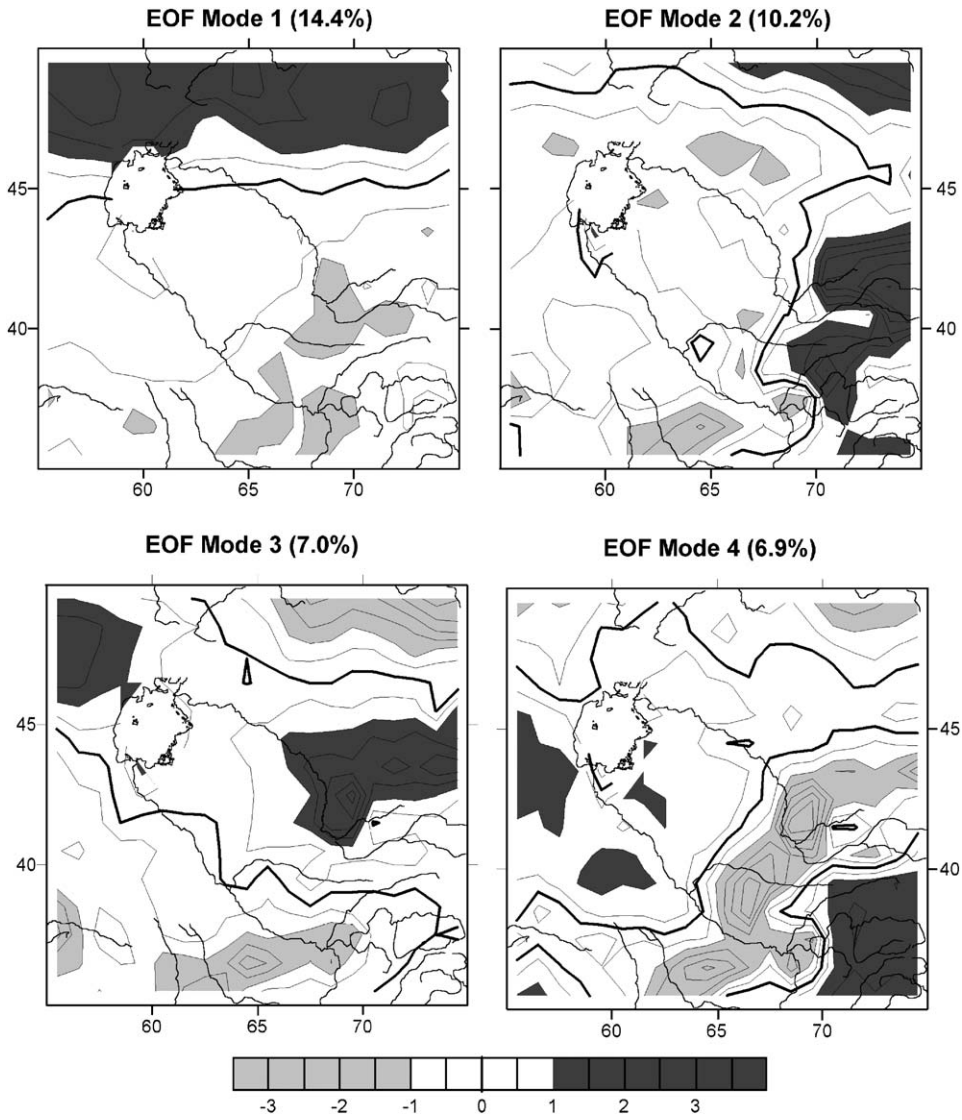

Fig. 5. Spatial distribution of four leading NDVI EOF modes.

analysis reveals two-year periodicity. Time-series exhibits no evident trend by 1990, followed by persistent period of negative EOF values in 1991–1994. In 1994–1997 the range of variations of the third EOF mode was wider then before 1994: very low value in the beginning of 1994 was followed by pronounced high value in the second half of 1994; the persistent low value during 1996 was followed by high value in 1997.

The fourth NDVI EOF mode explains 6.9% of variability. Its maximum is associated with high vegetation index on Pamir Mountains and on the Ustyurt

Table 1
Linear trends of the time series of the first four EOF modes of NDVI vegetation index and GPCP atmospheric precipitation

EOF mode	Coefficients of equation $Y = A + B \times t$ (Y—EOF mode; t—year)		Coefficient of determination R^2
	A	B	
NDVI-1	16.206557	−0.008142	0.0158
NDVI-2	−33.727029	0.016936	0.0962
NDVI-3	−11.895121	0.005969	0.0175
NDVI-4	34.934351	−0.017537	0.1525
GPCP-1	−18.394332	0.009248	0.0118
GPCP-2	48.982687	−0.024543	0.1104
GPCP-3	4.027986	−0.002020	0.0008
GPCP-4	76.558927	−0.038393	0.4060

Plateau and low NDVI in the upper courses of Murgab, Amu Darya, Zeravshan and Syr Darya Rivers (Fig. 5). The maximum periodicity of temporal oscillations is five years or more (Fig. 6d). An apparent decreasing trend was observed (Table 1); it was especially pronounced from 1983 till 1995. During that period vegetation was reduced in Pamir Mountains and increased in the upper courses of Amu Darya and Syr Darya.

The first GPCC EOF mode explains 15.6% of total variability. High NDVI values were observed to the north of the Aral Sea, with low NDVI values in the upper courses of Amu Darya, Syr Darya, and their tributaries (Fig. 7). We suppose that this EOF mode indicates negative correlation between precipitation in the northern and southern parts of the study region, related to large-scale process of atmospheric transport of moisture changing precipitation pattern. There was a slightly increasing linear trend (Table 1; Fig. 8a). Fourier analysis revealed the dominance of long-term periodicity (five years and more). Minima were observed in 1987, 1994, and 1998, maxima in 1989, 1992, 1996, and 2000.

The second GPCC EOF mode explains 11.7% of precipitation variation. High values were located in the southern part of the study region: in Kopet-Dag Mountains, in the basins of Tedjen and Murgab Rivers, and in a small area in the upper course of Amu Darya. Negative values of this EOF mode were located in the northeastern part of the study region, in Muyunkum Desert, and in Hindu Kush Mountains (Fig. 7). There was a decreasing linear trend (Table 1; Fig. 8b). The maximum spectral density revealed by Fourier analysis was three years. After a persistent period of high EOF mode in 1991–1992 it decreased; from 1992 to 1996 precipitation decreased in the southern part of the study region and increased in the Hindu Kush Mountains and in Muyunkum Desert. In 1996 a persistent period of low second GPCC EOF mode occurred, then from 1996 to the end of 1997 it increased, and during 1998 again decreased to negative values.

The third GPCC EOF mode explains 10.7% of precipitation variability. Its maximum was located in the upper course of Syr Darya and in Muyunkum Desert

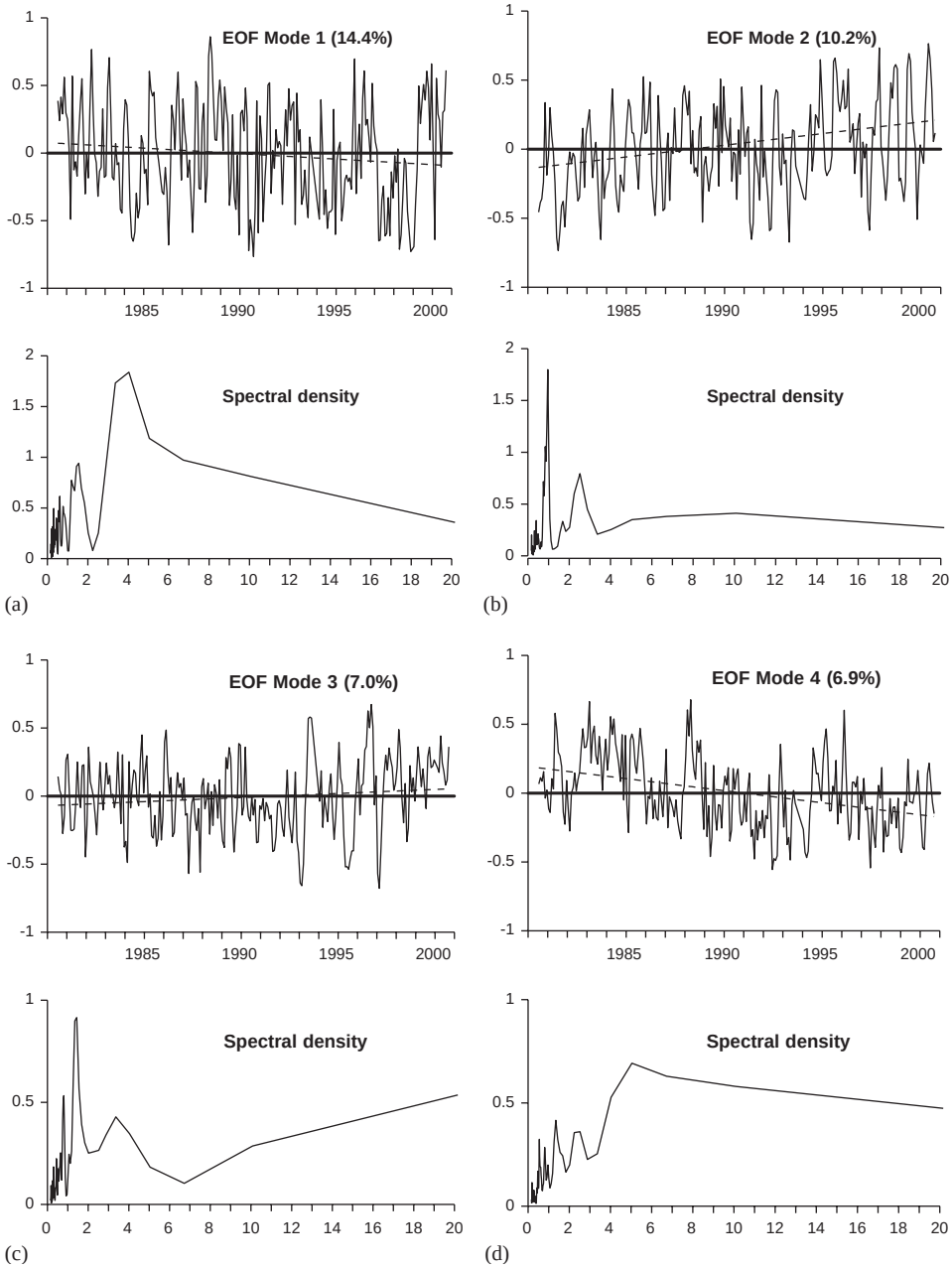

Fig. 6. (a) Temporal variations and spectral densities of the first NDVI EOF mode (explains 14.4% of total variability); (b) Temporal variations and spectral densities of the second NDVI EOF mode (explains 10.2% of total variability); (c) Temporal variations and spectral densities of the third NDVI EOF mode (explains 7.0% of total variability); (d) Temporal variations and spectral densities of the fourth NDVI EOF mode (explains 6.9% of total variability). Dashed lines indicate linear trends.

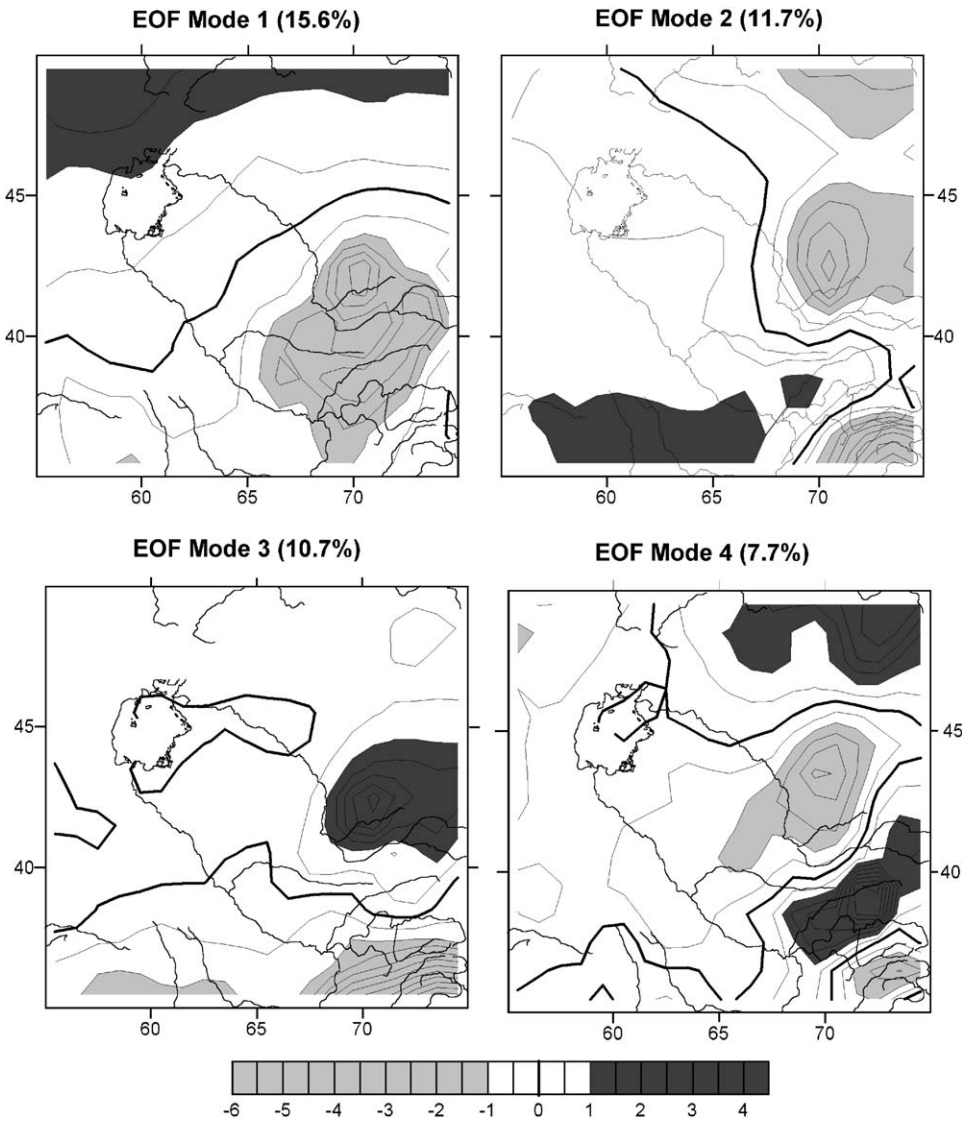

Fig. 7. Spatial distribution of four leading EOF modes of precipitation.

and minimum in the southern part of Pamir and Hindu Kush Mountains (Fig. 7). The linear trend was almost zero (Table 1; Fig. 8c). Long-term periodicity dominated, with maximum three years or more. A slight decreasing trend was observed from 1990 to 1995 with minimum in 1995–1996; then the third EOF mode increased.

The fourth GPCC EOF mode explains 7.7% of total variability in precipitation. The maximum values were located in the eastern Tien Shan and northern Pamir

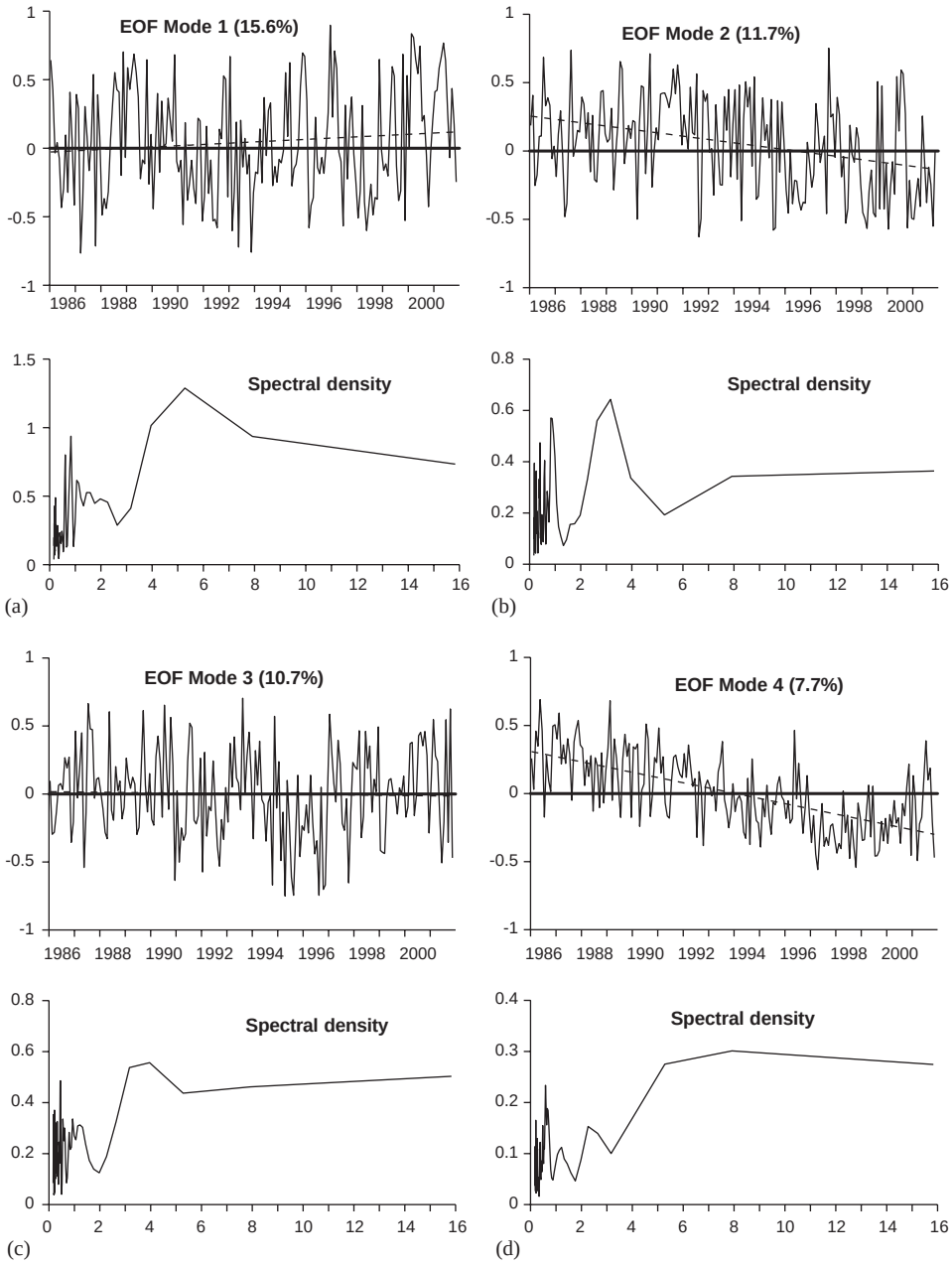

Fig. 8. (a) Temporal variations and spectral densities of the first EOF mode of precipitation (explains 15.6% of total variability); (b) Temporal variations and spectral densities of the second EOF mode of precipitation (explains 11.7% of total variability); (c) Temporal variations and spectral densities of the third EOF mode of precipitation (explains 10.7% of total variability); (d) Temporal variations and spectral densities of the fourth EOF mode of precipitation (explains 7.7% of total variability). Dashed lines indicate linear trends.

Mountains and in Ferganskaya Valley, and in the northeastern part of the study region. Minimum values were located in Muyunkum Desert and in the middle course of Syr Darya (Fig. 7). The linear trend was negative (Table 1; Fig. 8d). The maximum spectral density value exceeds five years. A gradual decrease is evident from 1986 till 1998, followed by the trend toward increase.

The following conclusions are derived from the analysis of four leading EOF modes of NDVI and GPCC:

Both first leading EOF modes of NDVI and GPCC exhibit similar spatial patterns, with positive extremes in the latitudinal zone to the north of the Aral Sea and negative extremes in the upper courses of Amu Darya, Syr Darya and their tributaries. Moreover, some features of temporal variation in these modes were similar: both modes had maxima in 1989 and 1996–1997, decreased from 1997 to 1998, and then increased again. Here we see a large-scale inter-annual correlation between precipitation and the vegetation index related to the transport of atmospheric moisture between zones located to the north and to the south of the Aral Sea.

The second and fourth GPCC EOF modes exhibited a decreasing trend, the second NDVI EOF mode tends to increase and the fourth NDVI EOF mode tends to decrease during the entire period of observations. In general, these trends describe an increase in precipitation in the Muyunkum Desert and in the most southeastern part of the study region (the eastern Hindu Kush). At the same time, precipitation decreased in the upper course of Amu Darya and to a lesser extent in Ferganskaya Valley and eastern Tien Shan. As for long-term trends in vegetation revealed by the second and fourth NDVI EOF modes, we observed an increase in the zones where the second NDVI EOF mode is positive and the fourth NDVI EOF mode is zero or negative (i.e., in the Muyunkum Desert). An opposite trend (zero or a decrease in the second and zero or an increase in the fourth NDVI EOF modes) was observed in the Kara-Kum and Kyzyl-Kum Desert regions along the lower courses of Amu Darya and Syr Darya Rivers. We speculate that the redistribution of precipitation from Ferganskaya Valley and surrounding Pamir and Tien Shan Mountains (where the flows of Amu Darya and Syr Darya are formed) to Muyunkum Desert results in more vegetation in Muyunkum Desert and less vegetation in the desert regions located around the Aral Sea.

4.3. Time-lagged correlation between NDVI and GPCC anomalies

In addition to the analysis of long-term inter-annual variability, it is important to understand time-lagged correlations between vegetation and precipitation anomalies (i.e. the response of vegetation to variation in precipitation during several subsequent months). In this section we analyse anomalies rather than total values. An anomaly is when there a difference between the actual total value and the seasonal climate data. A time lag was analysed over the period not exceeding 1 year. We estimated time-lagged correlations between four leading EOF modes of NDVI and four leading EOF modes of GPCC precipitation (Fig. 9). Below we use the terms NDVI and GPCC with subscript indices indicating the leading EOF modes. Most

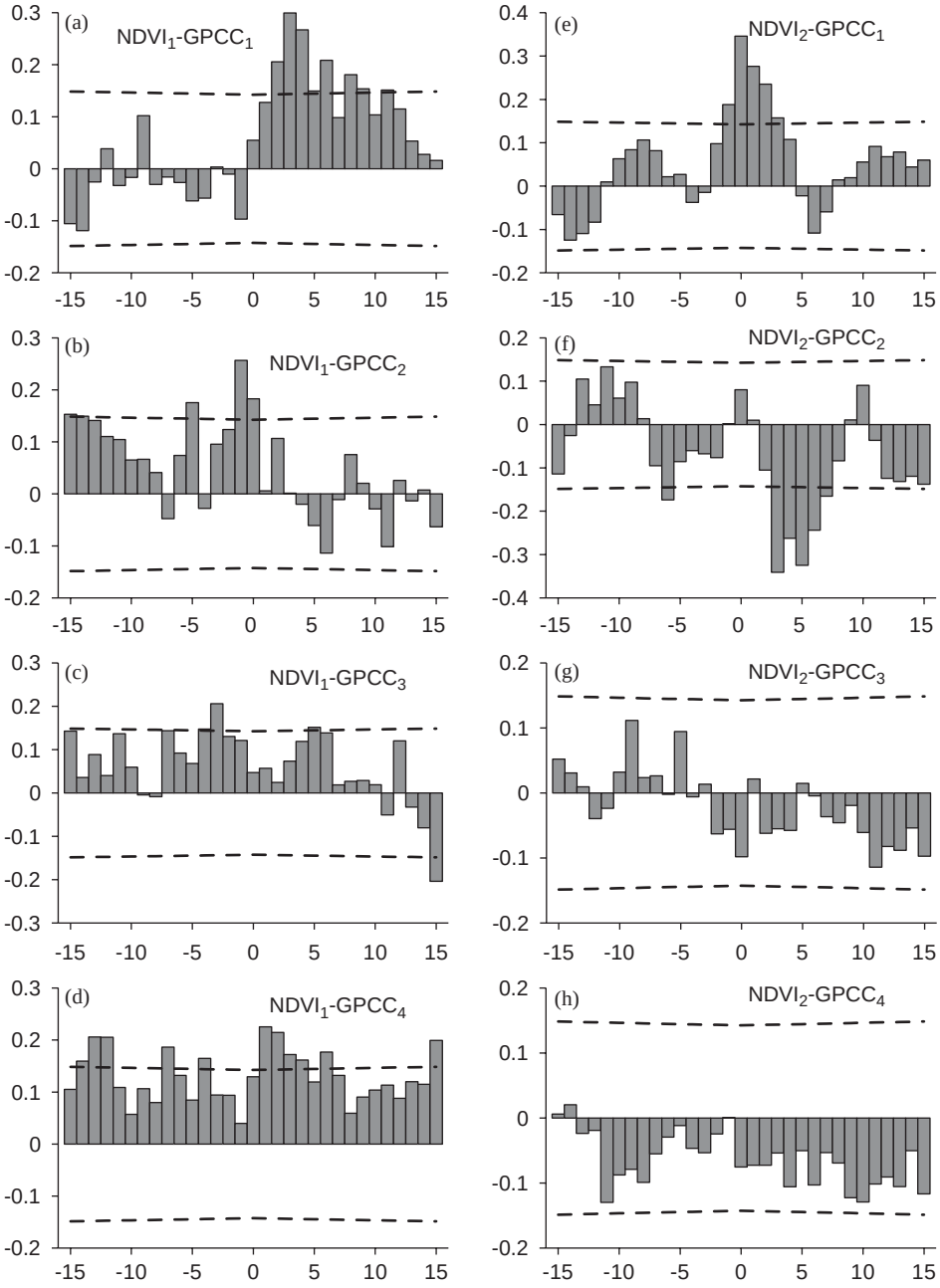

Fig. 9. Cross-correlation between four leading NDVI EOF modes ($NDVI_1$–$NDVI_4$) and four leading EOF modes of precipitation ($GPCC_1$–$GPCC_4$). Dashed lines indicate 95% confidence level.

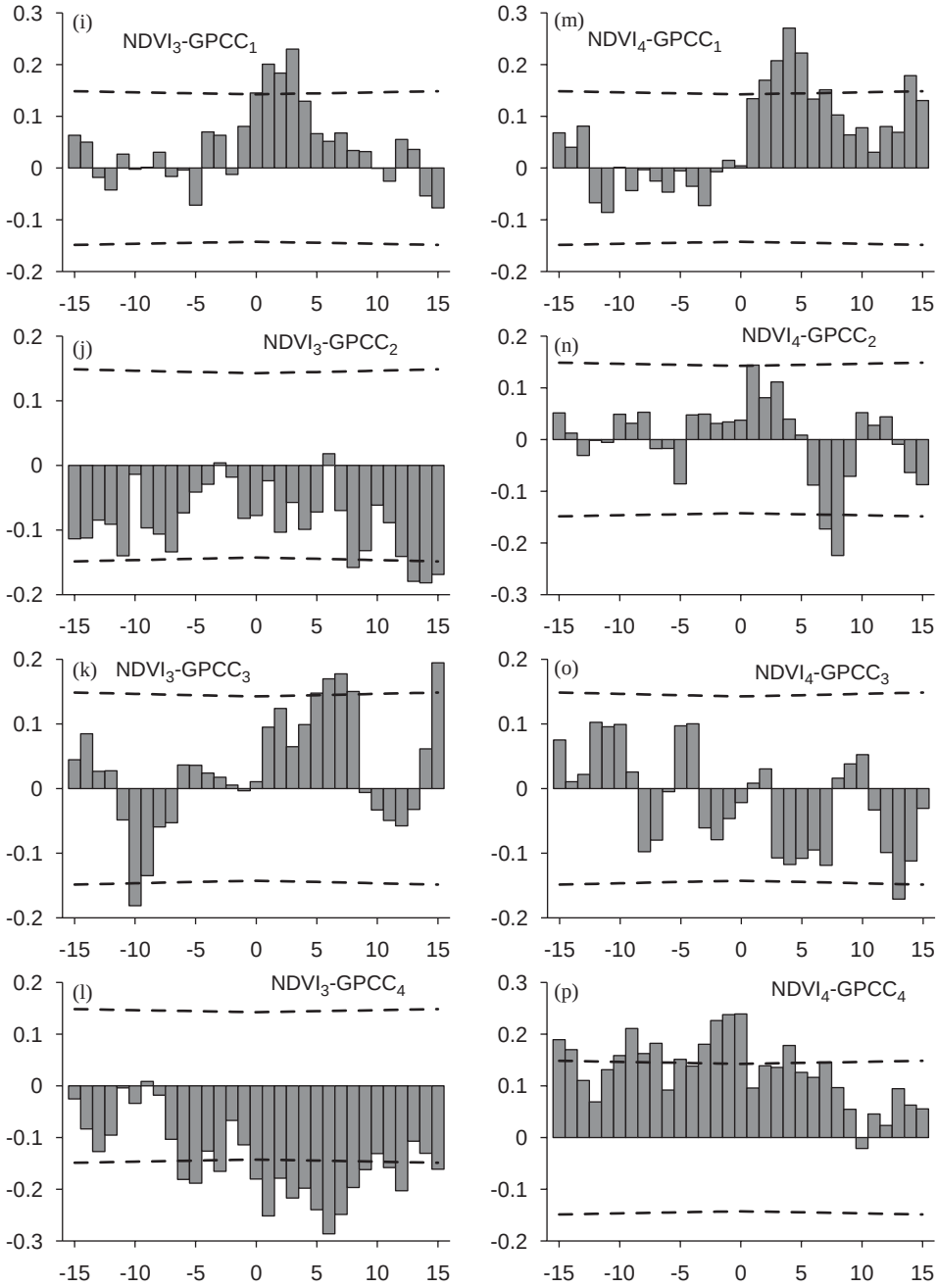

Fig. 9. (*Continued*)

combinations of GPCC and NDVI EOF modes exhibit a clear correlation, with precipitation leading vegetation index from 0 to 6 months. The difference between the time lags is of special interest and can be explained by different types of vegetation (desert, steppe, etc.).

Both leading EOF modes of vegetation index and precipitation ($NDVI_1$ and $GPCC_1$) were positively correlated with time lag of 3–4 months (Fig. 9a); NDVI values to the north of the Aral Sea and in the upper courses of Amu Darya and Syr Darya Rivers were positively correlated with precipitation observed in that region 3–4 months earlier. This time lag results from the well-known difference between the seasonal patterns of precipitation (maximum in spring) and vegetation (maximum in summer); more precipitation in spring results in more vegetation growth during the subsequent summer.

We do not have an explanation for the relationship between the first NDVI and the second GPCC EOF modes (Fig. 9b). $NDVI_1$ is positively correlated with $GPCC_2$, but NDVI (vegetation index) was 1 month ahead of precipitation. During the years when maximum precipitation was shifted from the eastern part of the study region to its southern part (see Fig. 7) NDVI was higher in the northern zone and lower in the upper courses of Amu Darya and Syr Darya Rivers (see Fig. 5). No explainable correlation within 1-year time lag was observed between $NDVI_1$ and $GPCC_3$.

$NDVI_1$ and $GPCC_4$ were positively correlated, with precipitation maxima preceding the vegetation index by 1–2 months (Fig. 9d). This correlation is related to the coincidence of the zones of positive EOF modes in the northeastern part of the study region, and the zones of negative EOF modes in the upper course of Syr-Darya and its tributaries. This regularity reveals short-scale relationship between rains and vegetation in steppe and desert zones, where rains are usually followed by plant growth 1–2 months later.

$NDVI_2$ and $GPCC_1$ exhibited a significant positive correlation with zero time lag (Fig. 9e). The positive zones of EOF modes coincide only in the northeastern part of the region (i.e. in the steppe zone) rather than in the zone of Aral Sea itself and the rivers flowing into it (i.e. in the desert zone). This correlation indicates an immediate response of vegetation to rain events in the steppe zone and the absence of this response in the desert zone surrounding the Aral Sea.

$NDVI_2$ and $GPCC_2$ are negatively correlated, precipitation being 3–5 months ahead of the vegetation index (Fig. 9f). The explanation is clear: the positive NDVI EOF_2 zone in the upper course of Syr Darya partly coincides with the negative GPCC EOF_2 zone, and the negative NDVI EOF_2 zones in the south and the small zone in the upper course of Amu-Darya coincide with the positive EOF_2 zones of GPCC EOF_2 mode. More precipitation in these regions in winter–spring results in a higher vegetation index 3–5 months later, in summer–autumn.

No explainable correlations were revealed between $NDVI_2$ and $GPCC_3$ (Fig. 9g), between $NDVI_2$ and $GPCC_4$ (Fig. 9h), between $NDVI_3$ and $GPCC_2$ (Fig. 9j), between $NDVI_4$ and $GPCC_2$ (Fig. 9n), and between $NDVI_4$ and $GPCC_3$ (Fig. 9o).

$NDVI_3$ and $GPCC_1$ were positively correlated; precipitation was 1–3 months ahead of the vegetation index (Fig. 9i). Positive zones of EOF modes coincided only

in the zone to the northwest of the Aral Sea. In the upper course of Syr Darya the zone of positive $NDVI_3$ coincided with the zone of negative $GPCC_1$; the correlation between precipitation and the vegetation index in this region is negative.

$NDVI_3$ and $GPCC_3$ were positively correlated, precipitation being 6–7 months ahead of the vegetation index (Fig. 9k). Positive zones of EOF modes coincide in the upper course of Syr Darya and in Muyunkum Desert to the north of Tien Shan Mountains. The $NDVI_3$ positive zone was located lower along the course of Syr Darya as compared with the $GPCC_3$ positive zone. It is reasonable to suggest that this correlation reflects the process of water accumulation in the ground and in the Syr Darya river bed during winter and spring; this accumulation results in a higher vegetation index in summer and autumn.

$NDVI_3$ and $GPCC_4$ were negatively correlated, the response of the vegetation index following precipitation within a wide range of time lags (1–7 months) (Fig. 9l). This correlation is in accord with the correlation between $NDVI_3$ and $GPCC_3$. The positive zone of $NDVI_3$ in the middle course of Syr Darya coincides with the negative zone of $GPCC_4$ in the middle and upper course of Syr Darya. More precipitation in that zone results in higher vegetation index there and downstream during the whole vegetation growth period.

$NDVI_4$ and $GPCC_1$ were positively correlated, precipitation being 4–5 months ahead of the vegetation index (Fig. 9m). The negative $NDVI_4$ zone coincides with the negative $GPCC_1$ zone in the upper courses of Amu Darya and Syr Darya. More water in winter and spring results in higher vegetation index 4–5 months later in summer and autumn.

Finally, we failed to explain the correlation between $NDVI_4$ and $GPCC_4$ (Fig. 9p). The correlation is positive, but the precipitation maxima are 0–2 months after the vegetation index. We speculate that the dynamics of both precipitation and vegetation index are correlated to many environmental factors (temperature, solar radiation, wind, etc.) not considered in this study. The correlation between $NDVI_4$ and $GPCC_4$ seems to be nothing but a manifestation of the inter-annual variability of complex climatic conditions around the Aral Sea.

5. Discussion and conclusions

Both atmospheric precipitation and the vegetation index in the study region exhibit pronounced seasonal variation. The maximum in the vegetation index occurring in May–June is 2–3 months after the maximum in precipitation (Fig. 4). These seasonal patterns are typical of temperate latitudes and not discussed here. Seasonal anomalies attract more attention, because they reveal the response of the vegetation index to atypical (i.e. more wet or more dry) precipitation occurring during different years. The time lag between precipitation and the vegetation index anomalies varies within wide range (i.e. from zero to 6–7 months).

A short time lag (from 0 to 2 months) is typical of steppe regions in the Kazakhskiy Melkosopochnik (“small hills”) area, in the zone to the northwest of the Aral Sea, and in the upper course of Syr Darya. A longer time lag (3–4 months) is

typical of the entire northern steppe area, the upper course of Syr Darya, and, to much less extent, the upper course of Amu Darya. A pronounced time lag reflecting the response of the vegetation index to precipitation about half a year later (i.e. an increased vegetation growth in summer after increased precipitation in winter–spring) is typical of the area along Syr Dara, the zone of vegetation response located lower along the Syr Darya course as compared with the zone of precipitation.

The response of NDVI to rainfall events was noted in many arid regions (Tucker et al., 1983; Nicholson et al., 1990; Maselli et al., 1993; Bastin et al., 1995; Richard and Poccard, 1998; Schmidt and Karnieli, 2000; Fang et al., 2001). The correlation between precipitation and NDVI emphasizes, on the one hand, rainfall as a limiting factor for vegetation growth, and, on the other, NDVI as a good indicator of vegetation in arid zone. One of the reasons is the absence of dense trees and shrubs. Instead, a large part of the arid and semi-arid surfaces are covered by microphytic communities of small non-vascular plants. When biogenic soil crusts are wet, the NDVI value can reach 0.3 due to the photosynthetic activity of these small plants (Karnieli et al., 1996, 1999; Schmidt and Karnieli, 2000). At the same time, in a more humid natural environment where high canopy densities occur, NDVI is a less effective indicator of plant biomass (Nicholson et al., 1990).

High correlation between precipitation and NDVI vegetation index is observed in the steppe zone to the north of the Aral Sea, in the upper and middle course of Syr Darya, and in the area to the north of Syr Darya, including Muyunkum Desert. At the same time, to the southeast of the Aral Sea, especially along the lower course of Amu Darya, we found no correlations between precipitation and the vegetation index. The absence of correlations indicates that in that zone the rain and snow water does not accumulate in the ground and does not sustain the development of vegetation. We hypothesize that this difference between Amu Darya and other regions could be explained by the intensive irrigation in that region started in 1960s (Micklin, 2000); the most important human action in this zone was the construction of the Kara Kum Channel. This improper water management resulted in that the natural water from Amu Darya and its tributaries was dispersed in desert soil instead of flowing downstream toward the Aral Sea. The result was a desiccation of the Aral Sea and subsequent decrease of the sea area and volume. The absence of correlations between water precipitation and the vegetation index illustrates that water not only does not reach the Aral Sea, but also does not sustain vegetation growth along the lower course of Amu Darya. Water in this zone is lost to both natural vegetation and agriculture; this feature is a serious consequence of an anthropogenic catastrophe, which took place in that natural region during the second half of the 20th century (Micklin, 2004).

An inter-annual variability is evident from the EOF modes of atmospheric precipitation and vegetation index. The precipitation over the catchment area of Amu Darya gradually decreased during recent two decades (Nezlin et al., 2004). The second and fourth NDVI EOF modes also indicate a long-term trend of decreasing vegetation in the desert areas of Kara-Kum, Kyzyl-Kum, and Muyun-Kum. These regions are most vulnerable to desertification, which is a self-accelerating process, "feeding on itself", because soil deterioration results in the destruction of the

productive potential of land areas (see details in Biswas and Biwas (1980)). We also have to take into account that the shrinking of the area of the Aral Sea decreased the evaporation from its surface, which, in turn, decreased the precipitation over the areas located far from the sea; this feedback relation, however, is beyond the scope of our study.

Discussing the trends in atmospheric precipitation, we have to take into account that the number of rain-gauge stations in the sparsely populated Aral Sea area is small and the monthly precipitation values over wide areas were obtained by interpolation based on the data points located far apart. The location of some stations changed during 20 years, which may cause additional error. In future studies, this problem can be partly solved by using remotely sensed precipitation data (Huffman et al., 2002; Nezlin et al., 2004). However, the reliability of the latter data is still questionable.

The period analysed in this study (16 years of GPCC and 21 years of NDVI) is too short to reveal a significant correlation with the global climatological cycles observed in other regions of the world. However, some features of NDVI and GPCC cycles are related to inter-annual weather indices in other world areas. For instance, the minima of both NDVI and GPCC leading EOF modes in 1986–1987 and subsequent maxima in 1988–1989 coincide with the extremes of the North Atlantic Oscillation index (Rodwell et al., 1999) and the Global Mean Sea Surface Temperature Anomalies Index (Lau and Weng, 1999). The abrupt changes observed in two leading NDVI and two leading GPCC EOF modes in 1997–1998 could be associated with the strongest El Niño event in the 20th century (McPhaden, 1999). El Niño event is an extreme of the global ENSO (El Niño Southern Oscillation) meteorological cycle of 3–7 years periodicity; its center is located in tropical Pacific, but it influences weather all over the world (Compo et al., 2001; Diaz et al., 2001; McPhaden, 1999; Peel et al., 2002), including the regions in Central Asia such as the Caspian Sea and Volga River basin (Arpe et al., 2000). Other studies (Lyatkher, 2000; Shermatov et al., 2004) revealed significant correlation between evaporation over the Aral Sea and solar activity (the variations of the sunspot period) and explained it with the influence of heat transportation by the Gulf Stream flow in the Atlantic Ocean and changing the wind trend over the Caspian Sea. However, the mechanism of interaction between these long-term oscillations is still unclear and needs further analysis.

6. Summary

Two decades of variation in the index of vegetation (NDVI) derived from the satellite observations by AVHRR radiometers were analysed in conjunction with 16 years of precipitation data in the Aral Sea region. Both variables exhibited pronounced seasonal variation, with maximum precipitation in March and maximum NDVI in May–June. The spatio-temporal variations were analysed by the Empirical Orthogonal Functions (EOF) method and time-lagged correlations between the EOF modes. The regions of synchronous seasonal and inter-annual

variability of the vegetation index and precipitation were distinguished. At the seasonal scale, precipitation and vegetation were correlated with time lags from 0 to 6 months with peaks in plant growth following precipitation maxima. The absence of correlation between precipitation and NDVI in some regions around the Aral Sea indicates the lack of water for vegetation growth and the zones of desert.

Acknowledgements

The authors thank the NASA Distributed Active Archive Center at the Goddard Space Flight Center for the production and distribution of NDVI data, and Global Precipitation Climatology Centre in Germany (GPCC) for the production and dissemination of precipitation data. We also thank Cameron Barrows, Xiongwen Chen and Aaron Jenks for their comments on the draft version of this paper. Two anonymous reviewers provided helpful comments and their input is greatly appreciated. This study was supported in part by INCO-COPERNICUS grant ARAL-KUM, NATO Collaborative Linkage Grant, US National Science Foundation and the University of California Agricultural Experiment Station.

References

Arpe, K., Bengtsson, L., Golitsyn, G.S., Mokhov, I.I., Semenov, V.A., Sporyshev, P.V., 2000. Connection between Caspian Sea level variability and ENSO. Geophysical Research Letters 27, 2693–2696.

Bannari, A., Morin, D., Bonn, F., Huete, A.R., 1995. A review of vegetation indices. Remote Sensing Review 13, 95–120.

Bastin, G.N., Pickup, G., Pearce, G., 1995. Utility of AVHRR data for land degradation assessment: a case study. International Journal of Remote Sensing 16, 651–672.

Biswas, M.R., Biwas, A.K., 1980. Desertification. Pergamon Press, Oxford 523pp.

Boomer, I., Aladin, N., Plotnikov, I., Whatley, R., 2000. The palaeolimnology of the Aral Sea: a review. Quaternary Science Reviews 19, 1259–1278.

Buschmann, C., Nagel, E., 1993. In vivo spectroscopy and internal optics of leaves as basis for remote-sensing of vegetation. International Journal of Remote Sensing 14, 711–722.

Cihlar, J., St-Laurent, L., Dyer, J.A., 1991. Relation between the Normalized Difference Vegetation Index and ecological variables. Remote Sensing of Environment 35, 279–298.

Compo, G.P., Sardeshmukh, P.D., Penland, C., 2001. Changes of subseasonal variability associated with El Niño. Journal of Climate 14, 3356–3374.

Cracknell, A.P., 1997. The Advanced Very High Resolution Radiometer (AVHRR). Taylor & Francis, London 534pp.

Diaz, H.F., Hoerling, M.P., Eischeid, J.K., 2001. ENSO variability, teleconnections and climate changes. International Journal of Climatology 21, 1845–1862.

Elvidge, C.D., Chen, Z.K., 1995. Comparison of broad-band and narrow-band red and near-infrared vegetation indexes. Remote Sensing of Environment 54, 38–48.

Fang, J., Piao, S., Tang, Z., Peng, C., Ji, W., 2001. Interannual variability in net primary production and precipitation. Science 293, 1723a.

Froebrich, J., Kayumov, O., 2004. Water management aspects of Amu Darya. In: Nihoul, J.C.J., Zavialov, P.O., Micklin, P.P. (Eds.), Dying and Dead Seas. Climatic Versus Anthropic Causes. Kluwer Academic Publishers, Dordrecht, pp. 49–76.

Gitelson, A.A., Kaufman, Y.J., Stark, R., Rundquist, D., 2002. Novel algorithms for remote estimation of vegetation fraction. Remote Sensing of Environment 80, 76–87.

Gobron, N., Pinty, B., Verstraete, M.M., Widlowski, J.-L., 2000. Advanced vegetation indices optimized for up-coming sensors: design, performance, and applications. IEEE Transactions on Geoscience and Remote Sensing 38, 2489–2505.

Gutman, G.G., 1991. Vegetation indexes from AVHRR: an update and future prospects. Remote Sensing of Environment 35, 121–136.

Gutman, G.G., 1999. On the use of long-term global data of land reflectances and vegetation indices derived from the advanced very high resolution radiometer. Journal of Geophysical Research 104, 6241–6255.

Huffman, G.J., Adler, R.F., Morrissey, M.M., Bolvin, D.T., Curtis, S., Joyce, R., McGavock, B., Susskind, J., 2002. Global precipitation at one-degree daily resolution from multisatellite observations. Journal of Hydrometeorology 2, 36–50.

Jarsjo, J., Destouni, G., 2004. Groundwater discharge into the Aral Sea after 1960. Journal of Marine Systems 47, 109–120.

Justice, C.O., Townshend, J.R.G., Kalb, V.L., 1991. Representation of vegetation by continental data sets derived from NOAA-AVHRR data. International Journal of Remote Sensing 12, 999–1021.

Karnieli, A., Shachak, M., Tsoar, H., Zaady, E., Kaufman, Y., Danin, A., Porter, W., 1996. The effect of microphytes on the spectral reflectance of vegetation in semiarid regions. Remote Sensing of Environment 57, 88–96.

Karnieli, A., Kidron, G.J., Glaesser, C., Ben-Dor, E., 1999. Spectral characteristics of cyanobacteria soil crust in semiarid environments. Remote Sensing of Environment 69, 67–75.

Kaufman, R.K., Zhou, L., Knyazikhin, Y., Shabanov, N.V., Myneni, R.B., Tucker, C.J., 2000. Effect of orbital drift and sensor changes on the time series of AVHRR vegetation index data. IEEE Transactions on Geoscience and Remote Sensing 38, 2584–2597.

Keyser, D., Khabibullayev, A., Moustafaev, V., 1999. Research for rehabilitating the Aral Sea region. Nature and Resources 35, 26–37.

Khan, V.M., Vilfand, R.M., Zavialov, P.O., 2004. Long-term variability of air temperature in the Aral Sea region. Journal of Marine Systems 47, 25–33.

Lambin, E.F., Strahler, A.H., 1994. Change-vector analysis in multitemporal space: A tool to detect and categorize land-cover change processes using high temporal-resolution satellite data. Remote Sensing of Environment 48, 231–244.

Lau, K.-M., Weng, H., 1999. Interannual, decadal-interdecadal, and global warming signals in sea surface temperature during 1955–97. Journal of Climate 12, 1257–1267.

Lyatkher, V.M., 2000. Solar cycle length stochastic association with Caspian Sea level. Geophysical Research Letters 27, 3727–3730.

Maselli, F., Conese, C., Petkov, L., Gilabert, M.A., 1993. Environmental monitoring and crop forecasting in the Sahel through the use of NOAA NDVI data. A case-study: Niger 1986–89. International Journal of Remote Sensing 14, 3471–3487.

McPhaden, M.J., 1999. Genesis and evolution of the 1997–98 El Niño. Science 283, 950–954.

Micklin, P., 2000. Managing water in Central Asia. Royal Institute of International Affairs, London 72pp.

Micklin, P., 2004. The Aral Sea crisis. In: Nihoul, J.C.J., Zavialov, P.O., Micklin, P. (Eds.), Dying and Dead Seas. Climatic Versus Anthropic Causes. Kluwer Academic Publishers, Dordrecht, pp. 99–123.

Nezlin, N.P., Kostianoy, A.G., Lebedev, S.A., 2004. Interannual variations of the discharge of Amu Darya and Syr Darya estimated from global atmospheric precipitation. Journal of Marine Systems 47, 67–75.

Nicholson, S.E., Davenport, M.L., Malo, A.R., 1990. A comparison of the vegetation response to rainfall in the Sahel and East Africa, using Normalized Difference Vegetation Index from NOAA AVHRR. Climatic Change 17, 209–241.

Peel, M.C., McMahon, T.A., Finlayson, B.L., 2002. Variability of annual precipitation and its relationship to the El Niño-Southern Oscillation. Journal of Climate 15, 545–551.

Pinker, R.T., Laszlo, I., 1992. Global distribution of photosynthetically active radiation as observed from satellites. Journal of Climate 5, 56–65.

Priesendorfer, R.W., 1988. Principle Component Analysis in Meteorology and Oceanography. Elsevier Science, New York 425pp.

Rasmussen, M.S., 1997. Operational yield forecast using AVHRR NDVI data: reduction of environmental and inter-annual variability. International Journal of Remote Sensing 18, 1059–1077.

Richard, Y., Poccard, I., 1998. A statistical study of NDVI sensitivity to seasonal and interannual rainfall variations in Southern Africa. International Journal of Remote Sensing 19, 2907–2920.

Rodwell, M.J., Rowell, D.P., Folland, C.K., 1999. Oceanic forcing of the wintertime North Atlantic Oscillation and European climate. Nature 398, 320–323.

Rouse, J.W., Haas, R.H., Schell, J.A., Deering, D.W., Harlan, J.C., 1974. Monitoring the vernal advancements and retrogradation (greenwave effect) of nature vegetation. NASA/GSFC Final Report, NASA, Greenbelt, MD, 371pp.

Rudolf, B., Hauschild, H., Reiss, M., Schneider, U., 1992. Beiträge zum Weltzentrum fùr Niederschlagsklimatologie. Meteorologische Zeitschrift N.F. 1, 7–84.

Schmidt, H., Karnieli, A., 2000. Remote sensing of the seasonal variability of vegetation in a semi-arid environment. Journal of Arid Environments 45, 43–59.

Sellers, P.J., 1985. Canopy reflectance, photosynthesis and transpiration. International Journal of Remote Sensing 6, 1335–1372.

Shepard, D., 1968. A two-dimensional interpolation function for irregularly spaced data. 23rd ACM National Conference. Brandon/Systems Press, Princeton, NJ, pp. 517–524.

Shermatov, E., Nurtayev, B., Muhamedgalieva, U., Shermatov, U., 2004. Analysis of water resources variability of the Caspian and Aral sea basins on the basis of solar activity. Journal of Marine Systems 47, 137–142.

Small, E.E., Sloan, L.C., Nychka, D., 2001a. Changes in surface air temperature caused by desiccation of the Aral Sea. Journal of Climate 14, 284–299.

Small, E.E., Giorgi, F., Sloan, L.C., Hostetler, S., 2001b. The effects of desiccation and climate change on the hydrology of the Aral Sea. Journal of Climate 14, 300–322.

Tarpley, J.D., Schneider, S.R., Money, R.L., 1984. Global vegetation indices from NOAA-7 meteorological satellite. Journal of Climate Applied Meteorology 23, 491–494.

Tucker, C.J., 1978. Post senescent grass canopy remote sensing. Remote Sensing of Environment 7, 203–210.

Tucker, C.J., 1979. Red and photographic infrared linear combination for monitoring vegetation. Remote Sensing of Environment 8, 127–150.

Tucker, C.J., Vanpraet, C., Boerwinkel, E., Gaston, A., 1983. Satellite remote sensing of total dry matter production in the Senegalese Sahel. Remote Sensing of Environment 13, 461–474.

Tucker, C.J., Townshend, J.R.G., Goff, T.E., 1985. African land cover classification using satellite data. Science 227, 369–374.

Tucker, C.J., Fung, I.Y., Keeling, C.D., Gammon, R.H., 1986. Relationship between atmospheric CO_2 variations and a satellite-derived vegetation index. Nature 319, 195–199.

Walter, H., 1985. Vegetation of the Earth and Ecological Systems of the Geo-biosphere. Springer, Berlin 318pp.

West, N.E., 1983. Temperate Deserts and Semi-Deserts. Vol. 5. Ecosystems of the World. Elsevier Scientific Publishing Co, Amsterdam 522pp.

Willmott, C.J., Rowe, C.M., Philpot, W.D., 1985. Small-scale climate maps: a sensitivity analysis of some common assumptions associated with grid-point interpolation and contouring. The American Cartographer 12, 5–16.